Journal of Materials Science & Technology 31 (2015) 979–985

Contents lists available at ScienceDirect

Journal of Materials Science & Technology

journal homepage: www.jmst.org

Spin States of 2D Nanocomposites of Ni and V Nanoclusters on Hexagonal *h*-BN, BC_3 and Graphene

P. Avramov [1,*], A.A. Kuzubov [2,3], S. Sakai [4], S. Entani [4], H. Naramoto [4], N. Eliseeva [2]

[1] *Kyungpook National University, 1370 Sankyuk-dong, Buk-gu, Daegu 702-701, Republic of Korea*
[2] *Siberian Federal University, 79 Svobodniy av., Krasnoyarsk 660041, Russia*
[3] *L.V. Kirensky Institute of Physics SB RAS, Krasnoyarsk, Academgorodok 660036, Russia*
[4] *Advanced Science Research Center, Japan Atomic Energy Agency, 2-4 Shirakata Shirane, Tokai-mura, Naka-gun, Ibaraki-ken 319-1195, Japan*

ARTICLE INFO

Article history:
Available online 20 August 2015

Key words:
Electronic structure
Metal nanostructure
Nanocomposites
Graphene
h-BN
BC_3
Spin states

Atomic and electronic structures of adsorbed nickel and vanadium atoms and nanoclusters (Ni_n and V_n, $n = 1–10$) on hexagonal *h*-BN and BC_3 lattices were studied using DFT PBE/PBC/PW (Perdew–Burke–Ernzerhof potential of density functional theory/periodic boundary conditions/plane wave basis set) technique. For the sake of comparison the structure and properties of the same nanoclusters deposited on pristine graphene were calculated as well. It was found that for all types of supports an increase of *n* from 1 to 10 leaded to decrease of coordination types from η^6 to η^2 and η^1. The *h*-BN- and BC_3-based nanocomposites were characterized by high (up to 18 μ for Ni_{10}/BC_3) magnetic moments of the nanoclusters and featured by positive binding energies. The graphene-based nanocomposites revealed energetic stability and, in general, lower magnetic moments per unit cell. The direct potential energy barriers for migration of Ni η^2/η^2 and η^6/η^6 types of dimers on graphene were low (10.9–28.9 kJ/mol) with high reverse barriers for η^6/η^6 dimers, which favored dynamically equilibrated Ni clusterization on graphene.

1. Introduction

The 2D layered nanocomposites consisting of metal nanoclusters on free-standing or deposited graphene, *h*-BN or hexagonal BC_3 have attracted intensive interests because of their promising applications in nanoelectronics, nanospintronics, chemical catalysis and energy storage. Hexagonal 2D lattices of graphene[1], *h*-BN[2] and BC_3[3] are perfect 2D hexagonal substrates of one-atom thickness to create elements of nanoelectronics, nanospintronics and energy storage devices[4–6].

The structure and properties of deposited graphene on transition metal (TM) surface and TM adatoms on graphene were studied previously using theoretical and experimental methods, and well-arranged reviews can be found elsewhere (see, for example[7,8]). In comparison with graphene- and *h*-BN deposited on transition metal surfaces, the composites involving TM adatoms and their nanoclusters are much more attractive due to the perspectives of applications for nanospintronics and heterogeneous catalysis.

Several experimental studies of the formation of TM nanoclusters on graphene have been published up to date. The nucleated island density *n* was measured as a function of growth parameters for several kinds of transition metals[9] with specifically high *n* for Fe nanoclusters. It increases continuously with the deposited amount and shows no temperature-dependence. These unusual results indicate the presence of long-ranged repulsive interactions between the Fe adatoms. The adsorption of Au and Pt atoms and their dynamical behavior on graphene have been also investigated in Ref. Gan et al. [10]. *In situ* experiments at 600–700 °C discovered the two-dimensional diffusion within the plane as well as the one-dimensional diffusion along the open edges (activation energies of 2.3–2.5 eV). It was shown that Au and Pt atoms strongly interact with carbon atoms of graphene. In the study of Fe, Gd, Dy and Eu on graphene, the 3D island growth morphology was commonly confirmed[11]. In contrast to Eu, upon thermal annealing, the Fe, Gd, and Dy nano-islands display a small decrease of island density and an increase of the height/width aspect ratio. The annealing of Eu islands at 365 K results in the formation of a close flat film. The structure and formation mechanisms of defect graphene-based nanocomposites with Fe, Co and Mo adatoms were experimentally studied by scanning transmission electron microscopy[12]. The 0.1 nm defects were created by focused electron beams to trap migrating Fe, Co and Mo atoms. It was found that single metal atoms or clusters could be localized in or on graphene layers.

Based on the investigation of the adsorption energies and diffusion barriers of the relevant metal adatoms on graphene using *ab initio* calculations[11], it was predicted that most of the

* Corresponding author. Ph.D.; Tel.: +82 53 9506342; Fax: +82 53 9506330.
E-mail address: paul@iph.krasn.ru (P. Avramov).

http://dx.doi.org/10.1016/j.jmst.2015.08.008

transition, noble and rare earth metals on graphene should exhibit a 3D growth. Most of the metal nanostructures on graphene should be also stable against the further aggregation. The Fe, Co, Ni, Pt, and Gd islands on graphene can serve as good candidates for surface-supported catalytic applications due to their 3D morphology and high thermal stability. The Zr/graphene binding energies were obtained in zirconium-coated graphene sheets at several coverages by employing *ab initio* calculations[13]. It was found that the increase of the Zr/C coverage ratio leads to the clusterization of Zr atoms. The Zr–graphene binding involves the charge transfer to graphene, which comes from the 5*s* orbital of Zr and also depends on the coverage ratio.

Extensive *ab initio* density-functional calculations were performed to investigate the structural, magnetic, and electronic properties of Ni_n and Fe_n nanostructures ($n = 1$–4) adsorbed on hydrogen passivated zigzag graphene nano-ribbons (ZGNR)[14]. It was found that both Ni and Fe atoms are strongly bound at ZGNR. The Ni_n nanostructures are more strongly bound than Fe_n nanostructures, and their atoms had much smaller spin magnetic moments. In particular, Ni_n/ZGNRs always have the lowest energy with antiparallel edge spins, whereas among Fe_n/ZGNRs only one- or two-atom adsorbed clusters are antiferromagnetic. A combined experimental (Scanning Tunneling Microscopy (STM), X-ray Absorption Spectroscopy (XAS), X-ray Magnetic Circular Dichroism (XMCD)) and theoretical (*ab initio* generalized gradient approximation (GGA) plane wave (PW)) study[15] of atomic structure and magnetic properties of TM_n/graphene/SiC(0001) nanocomposites (TM = Fe, Co, Ni; $n \geq 1$) reveals nonmagnetic ground state of single Ni and Co adatoms. Increasing of n ($n \geq 1$) leads to magnetic states for Ni_n nanoclusters up to 0.85 μ per each Ni atom. Ni/graphene nanocomposites with perfect and defect graphene have also been studied using theoretical approaches[16,17]. It was found that the defects in graphene lattice strongly affect the electronic structure and magnetic properties of the metal complexes, increasing the binding strength of the TM cluster on to the graphene substrate. Size-dependent atomic and electronic structures of a set of vanadium clusters V_n ($n = 2$–5) on graphene were studied using *ab-initio* GGA DFT (density functional theory) calculations[18]. It was discovered that low-dimensional V_n clusters are easily formed on graphene with nonmagnetic state as the most stable magnetic configuration.

In the present study, the atomic and electronic structures and spin states of a set of 2D TM_n/*h*-BN and TM_n/BC_3 (TM = Ni, V) complex nanocomposites were studied using the PW PBE (Perdew–Burke–Ernzerhof) electronic structure calculations within the periodic boundary conditions (PW PBE PBC). For the sake of comparison the TM_n/graphene nanocomposites were calculated using the same method of electronic structure calculations. It was found that in contrast with graphene-based nanocomposites, the formation of TM_n/*h*-BN and TM_n/BC_3 ones is endothermic process. The increase of the number of atoms in Ni_n nanoclusters leads to the increase of the magnetic moments per unit cell and the decrease of the coordination degree of nickel atoms. The formation of Ni nanoclusters on graphene proceeds through the migration of nickel adatoms across hexagonal lattice with the direct/reverse potential energy barriers of migration, 10.9–28.9/15.1–80.3 kJ/mol, through η^2-type transition states. The analysis of the density of states clearly demonstrates the spin polarization of the supports induced by adsorbed TM adatoms and nanoclusters.

2. Method of Electronic Structure Calculations and Nanocomposite Structure Models

To study the atomic and electronic structures of 2D nanocomposites, Kohn–Sham DFT PW basis sets, Projector Augmented Wave (PAW) formalism[19], Grimme correction of weak dispersion interactions[20] and PBE DFT potential[21] in PBC were used. For all calculations the cutoff energy (E_{cutoff}) was equal to 400 eV. The VASP code[22] was employed to perform all electronic structure calculations. The geometry of the nanocomposites was optimized until residual forces became less than 0.1 eV/nm. The Γ-centered Monkhorst–Pack[23] ($3 \times 3 \times 1$) *k*-point Brillouin zone sampling scheme was used. The binding energies of the nanocomposites were estimated using the following equation:

$$E_b = E_{TM/sup} - E_{TM} - E_{sup}$$

where E_b is the binding energy of a nanocomposite, $E_{TM/sup}$ is the total energy of TM/support nanocomposite, E_{TM} is the total energy of free-standing TM_n nanocluster and E_{sup} is the total energy of *h*-BN, BC_3 or graphene support.

The atomic hexagonal lattices of *h*-BN and graphene are well known and the detailed illustrations will not be shown for simplicity. For *h*-BN the $8 \times 8 \times 1$ supercell with $a = b = 1.9909$ nm translation vectors was used. For graphene, the same $8 \times 8 \times 1$ supercell of elementary hexagonal unit was employed with $a = b = 1.9690$ nm translation vectors. The BC_3 hexagonal lattice is presented in Fig. 1. The BC_3 unit cell consists of two types of hexagons C_6 and C_4B_2 with two different types of chemical bonds (C–C and B–C)[4]. To calculate the TM/BC_3 composites (TM = Ni, Co, V), the $4 \times 4 \times 1$ supercell with $a = b = 2.0577$ nm translation vectors was employed. To avoid unphysical interactions between the PBC partners, the vacuum interval along *c* direction was equal to 2.00 nm in all cases.

The process of clusterization of TM atoms on the substrates starts from adsorption of single adatoms and consecutive formation of dimers, trimers, etc. and, finally TM_n nanoclusters. To study the initial stages of clusterization, knowledge about the structure and spin states of single adatoms, dimers and trimers is important. As an example of larger clusters, the Ni_{10} and V_{10} which can be formed as single- and double-layered structures were studied as well. All possible initial types of coordinations and atomic configurations of TM_n ($n = 1, 2, 3, 10$) on graphene, *h*-BN and BC_3 substrates were optimized using electronic structure calculations, but only a few structures were located. All optimized final structures of the nanocomposites are discussed in the text below.

Here and thereafter, we denote the coordination of a metal adatom at a middle of a chemical bond of hexagonal support lattice as η^2 type of coordination (see, for example, Fig. 2). The η^6 type of coordination means a complex bond between the metal and the center of hexagonal fragments (C_6 for graphene, B_3N_3 for *h*-BN and C_6 and B_2C_4 for BC_3, respectively). And finally the η^1 type denotes the coordination by one atom of the hexagonal lattices under consideration. For *h*-BN and BC_3-based composites, the actual sites of η^1 type of coordination are marked by chemical symbol of host lattice atom. For example, the B:η^1 denotes the coordination either by boron of BC_3 or *h*-BN, whereas N:η^1 denotes coordination of an adatom by nitrogen of *h*-BN support. For bilayer clusters η^1/η^1 and η^1/η^6 notations denote the coordination of atoms of the first metallic layer at η^1 or η^6 sites and η^1 type of coordination of the atoms of the second layer.

3. Results

3.1. Single Ni and V adatoms on h-BN, BC_3 and graphene

The details of atomic and electronic structures of Ni and V adatoms on *h*-BN, BC_3 and graphene are presented in Table 1 and Figs. 2 and 3. It is found that all three hexagonal lattices feature the η^6 coordination type of the adatoms. In addition, Ni adatoms at N:η^1, B:η^1 for Ni/*h*-BN; Ni at C:η^1 for Ni/BC_3; Ni at η^2 for Ni/graphene and

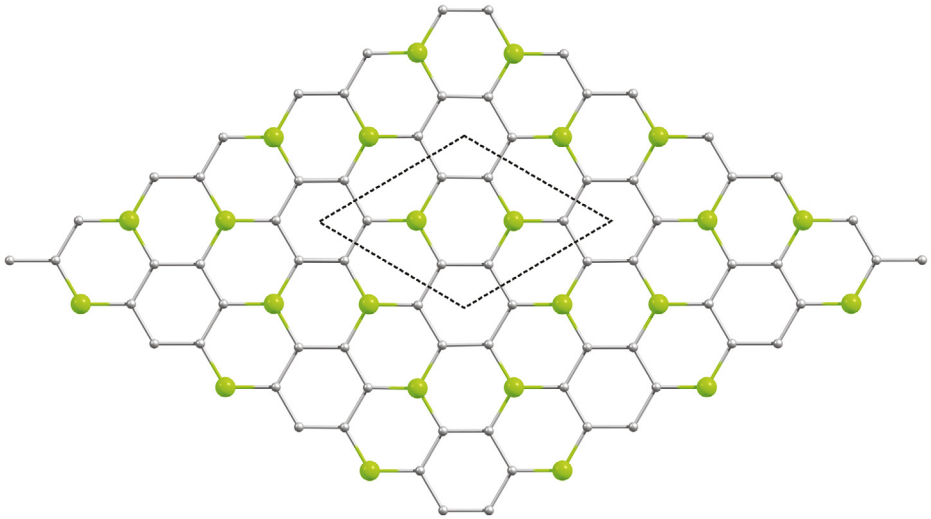

Fig. 1. Atomic lattice of BC_3. The boron atoms are presented in green, and the carbon atoms are presented in gray. The rhombus unit cell consists of two types of hexagons (C_6 and C_4B_2) as marked by dotted lines.

V at N:η^1, B:η^1 for V/*h*-BN are located. It is also found that vanadium adatoms exhibit high magnetic moments (up to 5 μ) for all hexagonal substrates, whereas Ni adatoms have weak magnetic moments of 0.138 μ especially for Ni/BC_3 C_6:η^6 configuration. All *h*-BN and BC_3 complexes with both Ni and V adatoms are featured by the positive binding energies.

The density of states and the spatial distribution of the spin density of V/graphene and Ni/graphene for comparison in η^6 configurations are presented in Fig. 4. The electronic structure of Ni/graphene complex is not spin-polarized, whereas the DOS of V/graphene is highly spin-polarized at the vicinity of the Fermi level. The difference in spin polarization can be easily realized referring to the spatial distribution of spin density (Fig. 4(b) and (c)). The V adatom spin density is positive in all supercell and mainly localized on V atom. For the Ni/graphene composite, the spin density with alternating signs is almost uniformly located on all atoms of the supercell. The integral spin density of Ni/graphene composite is equal to 0.

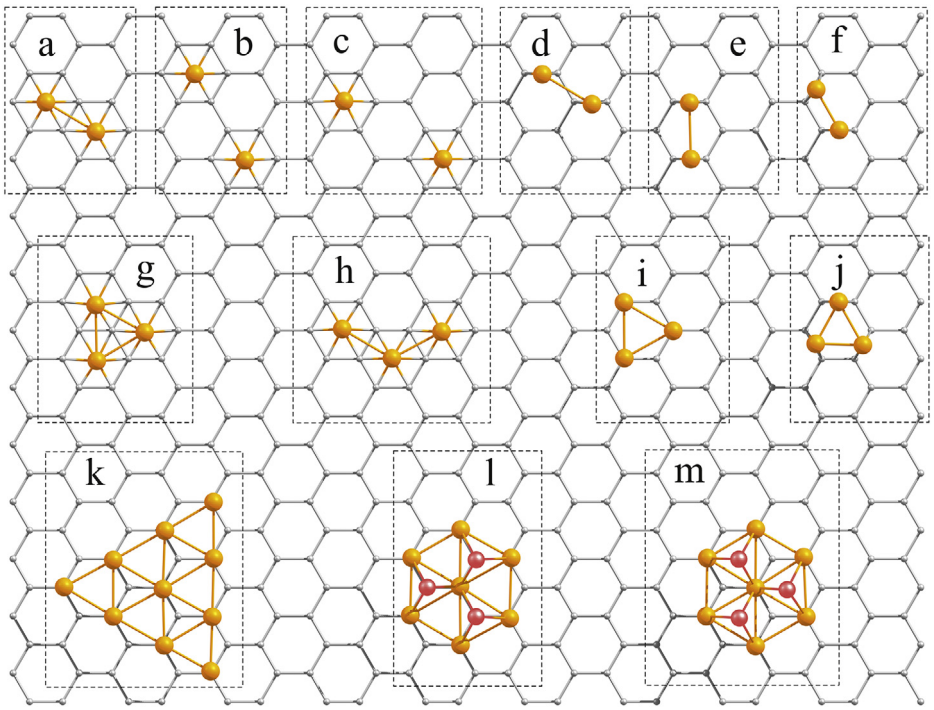

Fig. 2. (a, b, c) Atomic structures of two Ni adatoms on a hexagonal lattice in different η^6 positions. (d, e, f) Atomic structures of two Ni adatoms on a hexagonal lattice in different η^2 positions. (g, h) Atomic structure of Ni_3 nanocluster on a hexagonal lattice. The Ni adatoms are in η^6 positions. (i) Atomic structure of Ni_3 nanocluster on a hexagonal lattice. The Ni adatoms are in η^1 positions. (j) Atomic structure of Ni_3 nanocluster on a hexagonal lattice. The Ni adatoms are in η^2 positions. (k) Single-layered Ni_{10} nanocluster. The Ni adatoms are in η^1 positions. (l) Double-layered Ni_{10} nanocluster. Seven Ni adatoms of the first layer are in η^1 positions. Three Ni adatoms of the second layer are above η^1 positions. (m) Double-layered Ni_{10} nanocluster. Seven Ni adatoms of the first layer are in η^1 positions. Three Ni adatoms of the second layer are above η^6 positions. The carbon atoms are presented in gray, Ni atoms are presented in yellow (adatoms of the first layer) and orange (adatoms of the second layer).

Table 1
Atomic structure and magnetic moments of single adatoms on hexagonal lattices

Nanocomposite	Type of coordination	Binding energy (eV)	Magnetic moment per supercell (μ)	The distance from adatom to the closest atom of the surface TM–lattice atom distance (nm)	Shortest distance from adatom to the surface (nm)
Ni/graphene	η^2	−1.611	0.000	0.1941	0.1875
	η^6	−1.817	0.000	0.2113	0.1524
V/graphene	η^6	−1.232	4.066	0.2337	0.1806
Ni/*h*-BN	N:η^1	3.982	0.000	0.1882	0.1751
	B:η^1	4.007	0.000	0.1889	0.1723
	η^6	4.172	0.000	0.2122	0.1605
V/*h*-BN	N:η^1	4.581	5.000	0.2253	0.2207
	B:η^1	4.602	5.000	0.2282	0.2165
	η^6	4.788	5.000	0.2573	0.2075
Ni/BC_3	C:η^1	2.378	0.000	0.1878	0.1878
	C_6:η^6	2.120	0.138	0.2117	0.1553
	C_4B_2:η^6	1.878	0.000	0.2163	0.1554
V/BC_3	C_6:η^6	1.692	1.002	0.2109	0.1521
	C_4B_2:η^6	2.181	3.523	0.2264	0.1676

3.2. *Ni and V dimers on* h-*BN, BC_3 and graphene*

Electronic structure calculations reveal several possible Ni and V dimer configurations on *h*-BN and BC_3. The Ni dimers on *h*-BN are coordinated in η^1(N)/η^1(N) and η^6/η^6 (Fig. 2(a)) positions with 2.000 μ magnetic moments for both configurations (Table 2). The vanadium dimers are coordinated only in η^1(N)/η^1(N) positions with high 5.987 μ magnetic moment per supercell. The Ni_2 clusters on BC_3 are coordinated by $\eta^6(C_4B_2)/\eta^6(C_4B_2)$ and $\eta^6(C_4B_2)/\eta^6(C_6)$ (Figs. 1 and 2(a), Table 2) positions with 0 μ magnetic moments for both species. V dimers on BC_3 are characterized by the same $\eta^6(C_4B_2)/\eta^6(C_4B_2)$ and $\eta^6(C_4B_2)/\eta^6(C_6)$ (Figs. 1 and 2(a), Table 2) positions with high (3.345 and 4.948 μ, respectively) magnetic moments. All located dimer structures with *h*-BN and BC_3 are featured by positive binding energies regardless of the types of coordination of the adatoms (Table 2).

In comparison, several mutual coordinations of two nickel adatoms on graphene are located using electronic structure calculations (Table 2, Fig. 2) with Ni–Ni distances in the range of 0.2244–0.4945 nm. The atomic structure of Ni_2/graphene composites is a combination of η^2 and η^6 coordinations. Energetically preferable η^2/η^2 (Fig. 2(e)) configuration is characterized by the smallest Ni–Ni distance and the highest (2.0627 μ) magnetic moment for the supercell. The only one η^6/η^6 (Fig. 2(a)) V_2/graphene configuration with V–V distance of 0.2349 nm is located with the high (5.092 μ) magnetic moment.

Formation of the dimers leads to significant decreasing of averaged binding energies per adatom from approximately 4 eV for

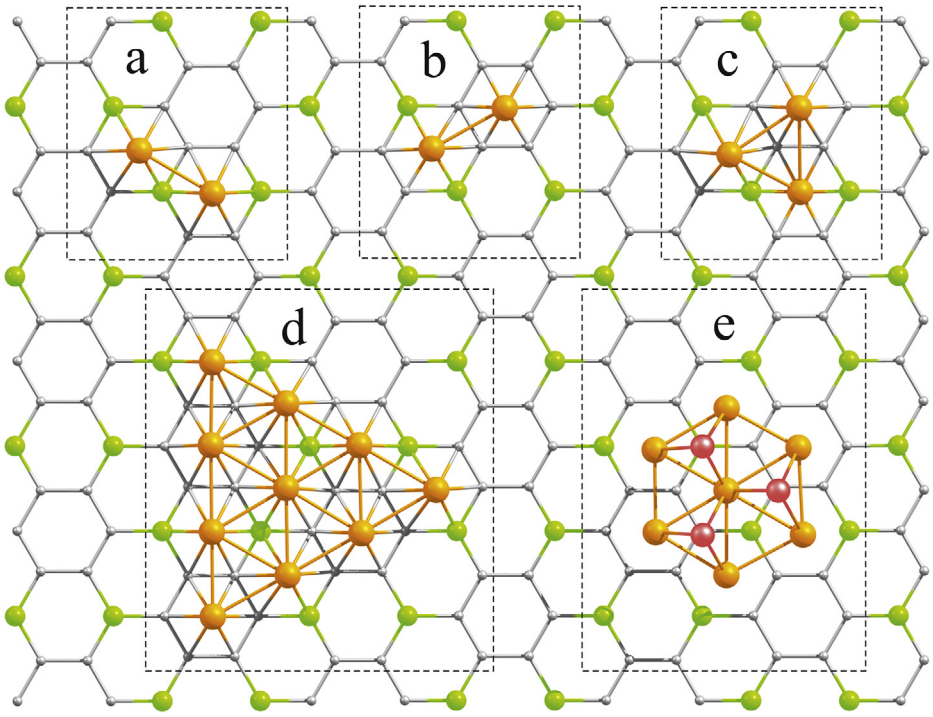

Fig. 3. (a, b) Atomic structure of two Ni adatoms on BC_3 in different η^6 positions. (c) Atomic structure of three Ni adatoms on BC_3 in different mutual η^6 positions. (d) Single-layered Ni_{10} nanocluster. The Ni adatoms are in η^6 positions. (e) Double-layered Ni_{10} nanocluster. Seven Ni adatoms of the first layer are in η^6 positions. Three Ni adatoms of the second layer are above C:η^1 (two atoms) and B:η^1 positions. The carbon atoms are presented in gray, boron atoms are presented in green, Ni atoms are presented in yellow (adatoms of the first layer) and orange (adatoms of the second layer).

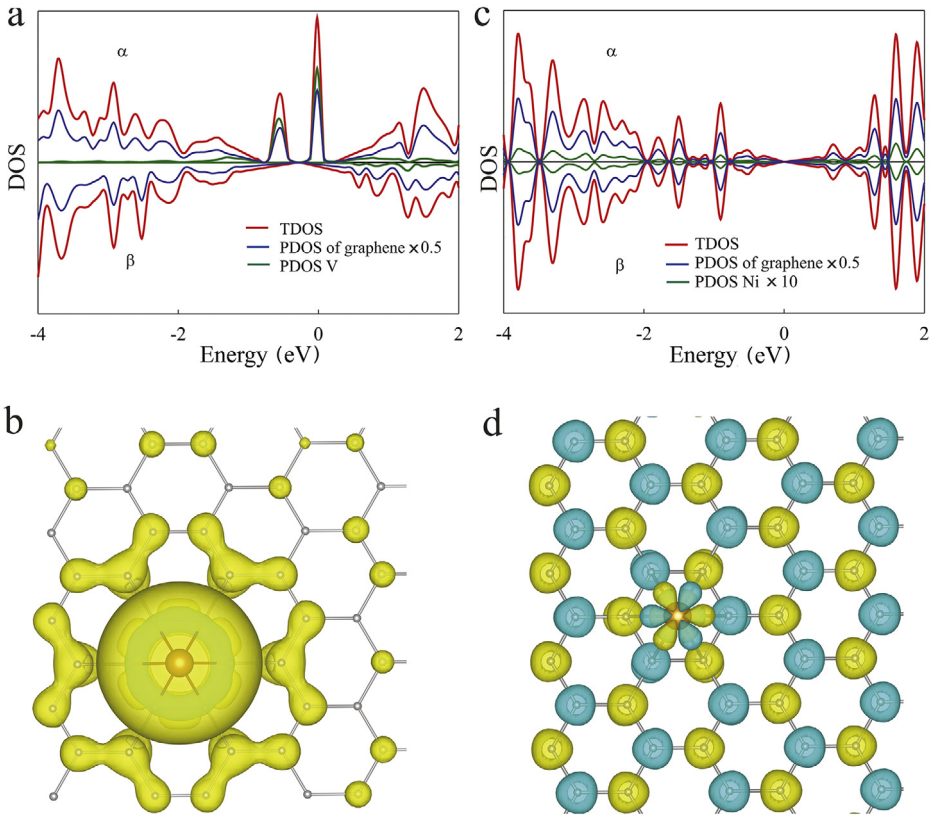

Fig. 4. Density of states and spatial distribution of spin density of V/graphene (a, b) and Ni/graphene (c, d) composites. The total densities of states (TDOS) are presented in red, the partial densities of states (PDOS) of graphene are presented in blue and PDOS of adatoms are presented in green for both composites. The positive partners of spin densities are presented in yellow and the negative ones are presented in blue.

Ni/*h*-BN heterostructures (Table 1) to 1.6 eV for Ni_2/*h*-BN. For V/*h*-BN–V_2/*h*-BN pair the decreasing of energy is also high: from approximately 4.6 eV (Table 1) to 2.0 eV per V adatom. Ni and V adatoms (Table 1) and dimers on BC_3 also demonstrate significant decreasing of the binding energies per atom from 2.2 eV to 0.9 eV and from 2.0 eV (averaged) to 1.0 eV, respectively. The decreasing of the binding energies can be attributed to formation of new metal–metal bonds between the metal atoms in the dimers. Because of significant decrease of binding energy per atom, formation of the dimers should increase the probability of formation of TM nanoclusters on *h*-BN and BC_3 supports.

3.3. *Ni and V trimers on BC_3, h-BN and graphene*

The features of atomic structure of Ni and V trimers on BC_3 and graphene lattices are presented in Table 3. In contrast with BC_3 and graphene, no specific atomic structures were located for Ni_3/*h*-BN and V_3/*h*-BN composites. The V_3/BC_3 composites of $\eta^6(C_4B_2)/\eta^6(C_4B_2)/\eta^6(C_6)$ type (Fig. 3(c)) reveal positive binding energy of 1.6 eV and relatively low (0.855 μ) magnetic moment per unit cell. No stable structures were detected for Ni_3/BC_3 nanocomposite either. Four complex Ni_3/graphene configurations were located by the electronic structure calculations. The most stable $\eta^2/\eta^2/\eta^2$ one (Fig. 2(j))

Table 2
Atomic structure and magnetic moments of Ni and V dimers on hexagonal lattices

Nanocomposite	Type of coordination	Binding energy (eV)	Magnetic moment per supercell (μ)	Maximum distance TM–C (nm)	Minimum distance TM–C (nm)	TM–TM distance (nm)	TM–surface distance (nm)
Ni_2/graphene	η^6/η^6 (Fig. 2(a))	–2.119	0.000	0.2174	0.2152	0.2401	0.1588
	η^6/η^6 (Fig. 2(b))	–1.812	0.000	0.2069	0.2154	0.4157	0.1541
	η^6/η^6 (Fig. 2(c))	–1.798	0.000	0.2118	0.2113	0.4945	0.1537
	η^2/η^2 (Fig. 2(d))	–2.083	1.5354	0.20991	0.1992	0.2280	0.1961
	η^2/η^2 (Fig. 2(e))	–2.137	2.0627	0.20648	0.2047	0.2244	0.1966
	η^2/η^2 (Fig. 2(f))	–2.126	1.726	0.2047	0.2039	0.2250	0.1972
V_2/graphene	η^6/η^6 (Fig. 2(a))	–1.232	5.092	0.2174	0.2152	0.2349	0.1796
Ni_2/*h*-BN	$\eta^1(N)/\eta^1(N)$	3.217	2.000	0.2581	0.2024	0.2236	0.1966
	η^6/η^6 (Fig. 2(a))	3.253	2.000	0.2959	0.2504	0.2142	0.2147
V_2/*h*-BN	$\eta^1(N)/\eta^1(N)$	4.034	5.987	0.2236	0.2236	0.2232	0.2178
Ni_2/BC_3	$\eta^6(C_4B_2)/\eta^6(C_4B_2)$ (Fig. 3(a))	1.777	0.000	0.2226	0.2209	0.2500	0.1535
	$\eta^6(C_4B_2)/\eta^6(C_6)$ (Fig. 3(b))	1.727	0.000	0.2246	0.2174	0.2373	0.1537
V_2/BC_3	$\eta^6(C_4B_2)/\eta^6(C_4B_2)$ (Fig. 3(a))	1.990	3.345	0.2394	0.2383	0.2204	0.1679
	$\eta^6(C_4B_2)/\eta^6(C_6)$ (Fig. 3(b))	1.890	4.948	0.2338	0.2332	0.2564	0.1744

Table 3
Atomic structure and magnetic moments of TM trimers on graphene and BC_3

Nanocomposite	Type of coordination	Binding energy (eV)	Magnetic moment (μ)	The shortest TM–C distance (nm)	TM–closest atom distance (nm)	Min TM–TM distance (nm)	Max TM–TM distance (nm)	Distance to support (nm)
Ni_3/graphene	$\eta^6/\eta^6/\eta^6$ (Fig. 2(g))	–2.879	2.189	2.076	2.046	2.282	2.273	2.035
	$\eta^6/\eta^6/\eta^6$ (Fig. 2(h))	–2.842	0.153	1.972	1.970	2.334	2.327	1.906
	$\eta^1/\eta^1/\eta^1$ (Fig. 2(i))	–2.758	0.386	2.268	2.162	2.440	2.438	1.562
	$\eta^2/\eta^2/\eta^2$ (Fig. 2(j))	–2.900	2.264	2.118	2.113	2.287	2.286	2.010
V_3/graphene	$\eta^6/\eta^6/\eta^6$ (Fig. 2(g)	1.437	5.544	2.404	2.313	2.416	2.425	1.836
V_3/BC_3	$\eta^6(C_4B_2)/\eta^6(C_4B_2)/\eta^6(C_6)$ (Fig. 3(c))	1.564	0.855	2.413	2.405	2.269	2.405	1.725

features the highest magnetic moment of 2.264 μ and short 0.2287 nm Ni–Ni distance. The V_3/graphene composite reveals high positive binding energies of 1.4 eV and high magnetic moment of 5.544 μ per unit cell. Like in the case of Ni and V dimers on *h*-BN and BC_3, the formation of V_3 nanoclusters on graphene and BC_3 also leads to decreasing of the binding energies per V atom up to 0.5 eV, further increasing the probability of formation of the V nanoclusters on both supports.

3.4. Ni_{10} and V_{10} nanoclusters on h-BN, BC_3 and graphene

The details of atomic structure of Ni_{10} and V_{10} nanoclusters on *h*-BN and BC_3 and graphene hexagonal lattices are presented in Table 4. Both single- and two-layered *h*-BN-based Ni_{10} and V_{10} nanocomposites are featured by positive formation energies and high magnetic states per unit cell. The single-layered Ni_{10}/*h*-BN nanocomposite reveals η^1(N) configuration of all Ni atoms with 2.2 eV binding energy and 6.368 μ magnetic moment per unit cell. Two-layered Ni_{10}/*h*-BN reveals η^1(N)/η^1 configuration and 1.8 eV binding energy with 5.845 μ per unit cell. The single-layered V_{10}/*h*-BN reveals η^1(N) type configuration of all atoms and 2.5 eV binding energy with 7.667 μ magnetic moment per supercell. Two-layered one has η^1(N)/η^1, 1.8 eV binding energy and 5.845 μ per unit cell.

The BC_3-based nanocomposites revealed the same types of coordination of Ni and V atoms in trimers. The Ni_{10}/BC_3 single-layered nanocomposite has $3\times\eta^6(C_6)/7\times\eta^6(C_4B_2)$ coordination (Fig. 3(d)), 1.225 eV binding energy and 18.322 μ magnetic moment per unit cell. The two-layered one has $2\times\eta^6(C_6)/5\times\eta^6(C_4B_2)/2\times\eta^1(C_6)/\eta^6(C_4B_2)$ (Fig. 3(e)), 1.164 eV and 0.232 μ per unit cell. The V_{10}/BC_3 single-layered $3\times\eta^6(C_6)/7\times\eta^6(C_4B_2)$ nanocomposite (Fig. 3(d)) has 1.4 eV binding energy and 1.069 μ magnetic moment per unit cell. Two-layered $2\times\eta^6(C_6)/5\times\eta^6(C_4B_2)/2\times\eta^1(C_6)/\eta^6(C_4B_2)$ one (Fig. 3(e)) is characterized by 1.1 eV binding energy and 4.130 μ magnetic moment per unit cell.

For heterostructures with positive binding energies, formation of Ni_{10} and V_{10} nanoclusters on graphene (for V_{10}), *h*-BN and BC_3 leads to reducing binding energies up to 0.1–0.2 eV per Ni and V atoms, making the clusterization of the nanoclusters much more probable.

The atomic structures of one single-layered and two bi-layered Ni_{10} nanoclusters deposited on graphene were located through the electronic structure calculations (Table 4). All nanoclusters have a tendency to be stabilized in low coordination state of η^1 as well as to form the bi-layered structures. The combined η^1/η^1 and η^1/η^6 coordination of bi-layered nanocluster was discovered to be the most energetically preferable nanocomposites. Both bi-layered and single-layered nanoclusters bear the high magnetic moments close to 6 μ per supercell, which is quite different from the case of small nickel clusters on graphene.

3.5. Ni dimer migration barriers on graphene

The Ni and V single adatom migration pathways on graphene and *h*-BN were recently studied[24]. In particular, it was found that in both cases the migration of the adatoms between η^6 equivalent minima undergoes through η^2 coordinations with the potential energy barriers of 19.2–33.9 kJ/mol. Because of that, only potential energy surfaces and mechanisms of Ni_2 dimer migration on graphene were studied with the final formation of η^2/η^2 (Fig. 2(e)) nickel dimer.

The energy difference between Ni_2/graphene η^6/η^6 (Fig. 2(a)) and η^2/η^2 (Fig. 2(e)) clusters is equal to 1.7 kJ/mol, which is comparable with the accuracy of DFT approach. Due to the very low energy difference between η^6/η^6 and η^2/η^2 Ni_2/graphene clusters, both isomers can co-exist. The transformation of η^2/η^2 isomer (Fig. 2(e)) from η^6/η^6 (Fig. 2(c)) can be kinetically affected by direct potential barrier of chemical reaction (28.9 kJ/mol). Another η^2/η^2 intermediate isomer (Fig. 2(d)) can be formed as well with the consequent transformation to η^2/η^2 dimer (Fig. 2(f)), and finally to η^2/η^2 dimer

Table 4
Atomic structure and magnetic moments of TM_{10} nanoclusters on graphene, *h*-BN and BC_3

Nanocomposite	Type of coordination	Binding energy (eV)	Magnetic moment (μ)	TM–closest atom distance (nm)	Min TM–TM distance (nm)	Max TM–TM distance (nm)	Distance to support (nm)
Ni_{10}/graphene	Single layer, η^1 (Fig. 2(k))	–3.5427	6.1192	0.19902	0.2290	0.2499	0.2015
	Two layers, η^1/η^1 (Fig. 2(l))	–3.7045	5.9570	0.20266	0.2309	0.2475	0.1992
	Two layers, η^1/η^6 (Fig. 2(m))	–3.7162	5.8996	0.20253	0.2314	0.2529	0.1990
V_{10}/graphene	Single layer, η^6	2.231	19.794	0.2272	0.2480	0.2711	0.1774
	Two layers, η^6/η^1	1.359	0.664	0.2245	0.2198	0.2626	0.1738
Ni_{10}/*h*-BN	Single, η^1(N)	2.158	6.368	0.2384	0.2028	0.3161	0.1965
	Two η^1(N)/η^1(B)	1.824	5.845	0.2107	0.2334	0.2444	0.1959
V_{10}/*h*-BN	Single, η^1(N)	2.518	7.667	0.2184	0.2156	0.2777	0.2006
	Two η^1(N)/η^1(B)	2.045	1.951	0.2051	0.2023	0.2671	0.1881
Ni_{10}/BC_3	Single layer, $3\times\eta^6(C_6)/7\times\eta^6(C_4B_2)$ (Fig. 3(d))	1.225	18.322	0.2063	0.2379	0.2491	0.1444
	Two layers, $2\times\eta^6(C_6)/5\times\eta^6(C_4B_2)/2\times\eta^1(C_6)/\eta^6(C_4B_2)$ (Fig. 3(e))	1.164	0.232	0.2103	0.2328	0.2533	0.1991
V_{10}/BC_3	Single layer, $3\times\eta^6(C_6)/7\times\eta^6(C_4B_2)$ (Fig. 3(d))	1.377	1.069	0.2.191	0.2.547	0.2.646	0.1.782
	Two layers, $2\times\eta^6(C_6)/5\times\eta^6(C_4B_2)/2\times\eta^1(C_6)/\eta^6(C_4B_2)$ (Fig. 3(e))	1.127	4.130	0.2.205	0.2.264	0.2.604	0.1.762

Table 5
Potential energy barriers of Ni dimer migration of graphene

Initial→final coordinations	ΔE (kJ/mol)	Direct potential barriers (kJ/mol)	Reverse potential barriers (kJ/mol)
η^6/η^6 (Fig. 2(b))→η^6/η^6 (Fig. 2(a))	–29.7	34.3 (η^2/η^2)	64.0 (η^2/η^2)
η^6/η^6 (Fig. 2(c))→η^6/η^6 (Fig. 2(a))	–31.0	18.8 (η^2/η^6)	80.3 (η^2/η^6)
η^2/η^2 (Fig. 2(d))→η^2/η^2 (Fig. 2(f))	–4.2	10.9 (η^1/η^2)	15.1 (η^1/η^2)
η^2/η^2 (Fig. 2(f))→η^2/η^2 (Fig. 2(e))	–1.2	23.8 (η^1/η^2)	24.7 (η^1/η^2)
η^6/η^6 (Fig. 2(c)) →η^2/η^2 (Fig. 2(e))	–32.6	28.9 (η^2/η^2)	61.5 (η^2/η^2)

(Fig. 2(e)) through 10.9 kJ/mol and 23.8 kJ/mol direct potential barriers, respectively. The reverse migration barriers of η^2/η^2 Ni dimers (Table 5, transformations Fig. 2(d)←Fig. 2(f) and Fig. 2(f)←Fig. 2(e), 15.1 kJ/mol and 24.7 kJ/mol, respectively) are also relatively small and should be dynamically equilibrated among the clusters.

The second type of η^6/η^6 dimer (Fig. 2(a)) can be formed through η^6/η^6 (Fig. 2(b)) and η^6/η^6 (Fig. 2(c)) isomers with 34.3 kJ/mol and 18.8 kJ/mol direct barriers, respectively. It was found that the structure of transition state for the η^6/η^6 (Fig. 2(b))→η^6/η^6 (Fig. 2(a)) transition is close to η^2/η^2 isomer (Fig. 2(d)). The second transition state was also formed by the displacement of one nickel atom toward the second one with the coordination just average between (η^2/η^6) and (η^2/η^2) isomers. The reverse barriers of η^6/η^6 (Fig. 2(a)) cluster formation from two η^6/η^6 (Fig. 2(b)) configurations are much higher (64.0 kJ/mol and 80.3 kJ/mol, respectively), which makes the nickel atom clusterization on graphene favorable.

4. Conclusion

Comparative DFT study of atomic and electronic structures of TM_n/*h*-BN, TM_n/BC_3 and TM_n/graphene nanocomposites (TM = Ni, V, n = 1, 2, 3 and 10) reveals the ability of nickel and vanadium to form different types of nanoclusters on *h*-BN, BC_3 and graphene with remarkable magnetic properties. Single TM adatoms prefer to occupy the η^6 coordination positions on all hexagonal lattices. The *h*-BN- and BC_3-based nanocomposites are characterized by high magnetic moments per unit cells (up to 18 μ) and, in contrast with graphene, positive binding energies. Increasing of the number of TM atoms in nanoclusters greatly decreases the binding energies per metal atom due to formation of new metal–metal bonds. This effect significantly increases the stability of the heterostructures and probability of their formation. The V_n/graphene nanocomposites have high (up to 5.1 μ) magnetic moments per unit cells. For Ni_n/graphene nanoclusters ($n > 1$) the η^6, η^2 and η^1 coordinations of nickel ions become competitive in energy. The higher the n number for Ni_n/graphene composites, the higher the magnetic moments per unit cell are observed. The direct potential energy barriers of nickel dimer migration pathways on graphene are low with the η^2-type transition states. For η^6/η^6 types of Ni dimers the reverse migration barriers become higher, which makes the nickel clusterization on graphene a favorable process.

Acknowledgments

The work of Russian team was supported by Russian Scientific Foundation (Grant No. 14-13-00139). P.V.A. acknowledges JAEA ASRC and Molecular Spintronics Group for hospitality and fruitful collaboration.

References

[1] K.S. Novoselov, A.K. Geim, S.V. Morozov, D. Jiang, Y. Zhang, S.V. Dubonos, I.V. Grigorieva, A.A. Firsov, Science 306 (2004) 666–669.
[2] R.W.G. Wyckoff, Crystal Structures 1, second ed., Interscience Publishers, New York, 1963, pp. 85–237. AMCSD database_code_amcsd 0011675.
[3] J. Kouvetakis, R. Kaner, M.L. Sattler, N.A. Bartlett, J. Chem. Soc., Chem. Commun. 24 (1986) 1758–1759.
[4] A.A. Kuzubov, A.S. Fedorov, N.S. Eliseeva, F.N. Tomilin, P.V. Avramov, D.G. Fedorov, Phys. Rev. B 85 (2012) 195415.
[5] J. Xue, J. Sanchez-Yamagishi, D. Bulmash, P. Jacquod, A. Deshpande, K. Watanabe, T. Taniguchi, P. Jarillo-Herrero, B.J. LeRoy, Nat. Mater. 10 (2011) 282–285.
[6] W. Auwärter, M. Muntwiler, J. Osterwalder, T. Greber, Surf. Sci. 545 (2003) L735–L740.
[7] Y.S. Dedkov, M. Fonin, New J. Phys. 12 (2010) 125004.
[8] D.S.L. Abergel, V. Apalkov, J. Berashevich, K. Ziegler, T. Chakraborty, Adv. Phys. 59 (2010) 261–482.
[9] S.M. Binz, M. Hupalo, X. Liu, C.Z. Wang, W.C. Lu, P.A. Thiel, K.M. Ho, E.H. Conrad, M.C. Tringides, Phys. Rev. Lett. 109 (2012) 026103.
[10] Y. Gan, L. Sun, F. Banhart, Small 4 (2008) 587–591.
[11] X. Liu, M. Hupalo, C.Z. Wang, W.C. Lu, P.A. Thiel, K.M. Ho, M.C. Tringides, Phys. Rev. B 86 (2012) 081414.
[12] J.A. Rodrıguez-Manzo, O. Cretu, F. Banhart, ACS Nano 6 (2010) 3422–3428.
[13] Y. Sanchez-Paisal, D. Sanchez-Portal, A. Ayuela, Phys. Rev. B 80 (2009) 045428.
[14] R.C. Longo, J. Carrete, J. Ferrer, L.J. Gallego, Phys. Rev. B 81 (2010) 115418.
[15] T. Eelbo, M. Wasniowska, P. Thakur, M. Gyamfi, B. Sachs, T.O. Wehling, S. Forti, U. Starke, C. Tieg, A.I. Lichtenstein, R. Wiesendanger, Phys. Rev. Lett. 110 (2013) 136804.
[16] W. Gao, J.E. Mueller, J. Anton, Q. Jiang, T. Jacob, Angew. Chem. Int. Ed. 52 (2013) 14237–14241.
[17] S. Sahoo, M.E. Gruner, S.N. Khanna, P. Entel, J. Chem. Phys. 141 (2014) 074707.
[18] Y. Zou, C.Y. Zhan, J.C. Wu, L.P. Zhou, H.X. Da, J. Kor. Phys. Soc. 63 (2013) 225–228.
[19] G. Kresse, J. Joubert, Phys. Rev. B 59 (1999) 1758–1775.
[20] S. Grimme, J. Comput. Chem. 27 (2006) 1787–1799.
[21] J. Heyd, G.E. Scuseria, M. Ernzerhof, J. Chem. Phys. 118 (2003) 8207–8215.
[22] G. Kresse, J. Hafner, Phys. Rev. B 49 (1994) 14251–14269.
[23] H.J. Monkhorst, J.D. Pack, Phys. Rev. B 13 (1976) 5188–5192.
[24] O.V. Yazyev, A. Pasquarello, Phys. Rev. B 82 (2010) 045407.